A generalized differential quadrature-based computational model for describing free vibrations behavior of functionally graded circular plates around buckled configuration

A. Shahabodini[a,*], M. Saadatmand[b], B. Ahmadi[c], S. Nezamivand Chegini[d]

[a]*Department of Mechanical Engineering, Vali-e-Asr University of Rafsanjan, Rafsanjan, Iran*
[b]*Laboratory Unit, Stam Sanat Company, Karaj , Iran*
[c]*Department of Mechanical Engineering, University of Kurdistan, Sanandaj, Iran*
[d]*Department of Mechanical Engineering, Ahrar Institue of Technology and Higher Education, Rasht, Iran*

Abstract. In the present article, the vibrational behavior of buckled functionally graded (FG) circular plates with clamped and simply-supported edge conditions is described. Considering von Kármán's assumptions, the geometric nonlinearity is incorporated into the Kirchhoff plate theory and the nonlinear governing equations of motion are then derived using Hamilton's principle. Critical buckling load and linear natural frequencies are first calculated using the generalized differential quadrature (GDQ) method. Afterward, the postbuckling characteristics of the circular plate are obtained via solving the nonlinear governing equations, directly. By several comparative studies, the reliability of the presented model is revealed. Finally, the fundamental natural frequency of the plate is evaluated for prebuckled and postbuckled configurations. The effects of material property and boundary conditions on the static bifurcation diagram and the natural frequency of the initial undeflected and bucked plate are studied. It is found that the trend of the fundamental natural frequency changes with the applied radial load around the prebuckled configuration is unlike the one around the buckled configuration.

Keywords: Free vibrations; Buckled circular plate; von Kármán's nonlinearity; *Functionally graded materials; generalized differential quadrature method*

Nomenclature

R	Plate radius
h	Plate thickness
r, θ and z	Coordinate variables in the radial, circumferential and thickness directions

[*]. *Corresponding author.*
E-mail addresses, Tel/Mobile number: a.shahabodini@vru.ac.ir, +98 34 31312565/+989132900948 (A. Shahabodini); s.miladsaadatmand@gmail.com, +989121642548 (M. Saadatmand); b.ahmadi.mech@gmail.com, +989189852881 (B.Ahmadi); saeed.nezamivand@gmail.com, +989112330254 (S. Nezamivand Chegini)

V_c and V_m	Volume fraction of ceramics and metal
E_c and E_m	Young's modulus of ceramics and metal
ρ_c and ρ_m	Mass density of ceramics and metal
ν	Poisson's ratio
u and w	Mid-plane displacement in the radial and thickness directions
ε_{ij}	Strain tensor
σ_{ij}	Stress tensor
λ and μ	Lamé constants
N_{r0}	External radial force
A_{11}, B_{11} and D_{11}	Stiffness coefficients
I_1, I_2 and I_3	Mass moments of inertia
N_r, M_r and M_θ	Resultant force and moments
n	Number of discrete points
$\mathbf{K}_L$ and $\mathbf{N}$	Conventional and geometric stiffness matrices
$\mathbf{D}^{(m)}$	Weighting coefficients matrix in differential quadrature method
$\mathbf{I}$	Identity matrix
c	Load control parameter
u_s and w_s	Displacement variables in postbuckling region
d_u and d_w	Time-dependent disturbances
ω	Natural frequency of vibration
δ_u and δ_w	Mode shapes of vibration
$\mathbf{M_L}$	Mass matrix
P_{crit}	Critical buckling load

1. Introduction

In 1984, a group of Japanese materials scientists put forward the idea of the construction of functionally graded materials (FGMs). The supreme properties of FGMs such as high thermal resistance and lack of

stress concentration make them a prime candidate for future smart composites in lots of engineering fields e.g., fast computers, aerospace and environmental sensors [1]. Regarding the increasing applicability of FGMs in practice, the mechanical behavior of FGM structures has been of a great interest for engineers. The buckling, postbuckling and vibration analyzes of the plate structures are of much importance in the design of FGMs devices. A lot of research works on these topics can be found in the literature. In the following, some of the most relevant published works on the static and vibrational analysis of FG (functionally graded) plates are cited.

Najafizadeh and Hedayati [2] studied axisymmetric buckling of FG circular plates subjected to thermal and mechanical loads. The authors derived governing equations according to the first-order shear deformation plate theory. A semi-analytical solution method was proposed by Allahverdizadeh et al. [3] to explore nonlinear free and forced vibration properties of a thin circular FG plate. The authors showed that the natural frequencies of the plate vary with vibration amplitudes and material gradient index. Sepahi et al. [4] investigated the buckling and postbuckling behavior of FG annular plates in thermal environment. The material properties were considered to vary in the radial direction. Fallah et al. [5] addressed the postbuckling behavior of functionally graded circular plates by applying an asymmetric load in the plane and transvers directions based on the first-order von Kármán theory. Ansari et al. [6] employed a variational method to present a weak solution of vibrations problem of nanocomposite oblique plates in thermal environment. Żur investigated the axisymmetric vibrations of functionally graded circular and annular plates utilizing Green's function method [7-9] and quasi-Green's function method [10]. The author [11] also developed closed-form multiparametric solutions for frequency analysis of FGM circular plates with porosity adopting classical plate theory. Shahabodini and his coworkers [12, 13] proposed a continuum model incorporating interatomic potential to address the vibration problems of nanoscale plates with small and large amplitude of oscillations. A review of advanced works on optimization of functionally graded materials up to 2018 was presented by Nikbakht and his co-workers [14]. The important findings of the research on different kinds of FG structures were explanied. Smita and Mohanty [15] developed a finite element model to treat the vibrations of a rotating FG plate subjected to thermal environment based on the higher-order shear deformation theory. Gholami and Ansari [16] investigated the free vibration behavior of postbuckled FG nanocomposite annular plates employing a numerical technique based on the differential quadrature. Arti and Shojaee [17] analyzed static, vibrational and buckling behavior of composite plates based on the coupling of truncated hierarchical B-splines and reproducing kernel particle method within higher-order shear deformation plate theory. Li et al. [18] successfully implemented a new generalized 5-variables theory accounting for shear deformation effect to calculate the static response of functionally graded plates. The authors considered the effect of volume fraction of constituent phases and aspect ratio on the static behavior. Sharma [19] did a study on free vibration of circular plate with piezoelectric layer

for fixed-fixed boundary condition using COMSOL multiphysics. In the paper published by Radaković et al. [20], thermal buckling and free vibration analyzes of FG plate were investigated. The authors defined a new shape function-based mathematical model of FG plate using higher-order shear deformation theory. Lal and Saini [21] examined vibrations of thin FG circular plates with parabolic variation of thickness in the radial direction when subjected to a thermal environment. Xu and Wellen [22] analytically derived duffing equations to investigate the effect of moderately large transverse load on the nonlinear dynamics of a circular plate with clamped edge support. They adopted harmonic balancing method to study the frequency response near the primary resonance. Imran et al. [23] conducted experimental, analytical and numerical simulations to treat the vibrations of composite plates using Rayleigh-Ritz and finite element methods. They found that increasing delamination size leads to decrease in the natural frequency. Qin et al. [24] considered a circular composite plate-type structure containing stiffener and studied its bending and vibration behaviors using a Mindlin's plate theory-based mesh-free method. The authors compared the results of their model with those of finite element method and found a superiority as it does not need any mesh in deriving governing equations of the members. Javani et al [25] adopted the first-order shear deformation theory along with the nonlinear kinematic relations to study the free vibrations of graphene platelet (GPL) reinforced composite circular plate. The plate was functionally graded in three types of distribution of GPL and lying on a nonlinear elastic foundation. The authors used the generalized differential quadrature (GDQ) and the weighted residual methods to calculate the natural frequencies of the nanocomposite. The circular and annular plates made of the same composite materials were treated by Sobhi [26] under mechanical and thermal loads, humidity as well as in-plane magnetic field. He developed a GDQ-based three-dimensional solution to determine the displacement and stresses within the plates. Hilali and Bourihane [27] combined the asymptotic numerical and the Hermite-Type moving least squares methods for the study of bending, buckling and postbuckling of classical thin plates. They also adopted the arc-length continuation technique to trace the solution path. Singh and Sahoo [28] proposed an analytical solution for determining the stresses and natural frequencies of FG carbon nanotubes reinforced plates. The solution was based on the trigonometric shear deformation theory and Navier's approach. In another work, Singh et al. [29] analyzed dynamic instability of the same structure when subjected to in-plane loading based on the higher-order shear deformation theory. They derived parametric relations for the stress components within the plate using Airy's stress function and determined the instability boundaries using Galerkin's and Bolotin's methods.

With the rapid progression in technology of structural elements, FG circular plates have wide applications in various technological situations and smart materials such as magneto-electro-elastic functionally graded plates and nano/micro electromechanical systems (NEMS/MEMS) [30, 31]. Furthermore, based on the literature review in both aspects of buckling and vibration analysis of circular FG plates, one can find that

there is a clear gap in the vibration analysis of buckled functionally graded circular plates. In all the aforementioned works, only the buckling or vibrational response of the plates was examined separately, and the dependence of these two phenomena and their effects on each other were not evaluated. While, as shown in Refs. [16, 32], the configuration (either the prebuckled or postbuckled one) may have significant effect on the vibrational behavior of the structure. Moreover, the effect of inertia and stiffness on the dynamics of the structure may be different when it vibrates around these two types of configuration. Prompted by this, the main goal of this paper is to evaluate the natural frequency of vibration of the FG circular plates around the buckled configuration and to examine whether the configuration affects on the role of stiffness and inertia in vibrations behavior of the structure as the characteristics of a vibratory system. To this end, the Kirchhoff plate theory for an axisymmetric analysis is used in conjunction with the von Kármán's assumptions to derive the nonlinear governing equations and boundary conditions of the FG circular plates. With the use of the GDQ method, the linear buckling and nonlinear postbuckling problems are first solved and the buckled configuration is described. Subsequently, the linear vibration of the prebuckled and postbuckled plate is investigated. Through a few comparative studies, the effectiveness of proposed approach is checked. Also, the effects of edge conditions, material gradient and radial force on the frequencies of the plate are studied. The formula derived in this paper can be efficiently applied to the axisymmetric analysis of vibrational behavior of the buckled FG circular plates.

2. Mathematical formulation

2.1. Modeling the material properties of FGM circular plate

A functionally graded circular plate of radius R and thickness h is considered in a cylindrical coordinate system (as shown in Fig. 1) that its origin is located at the center of mid-plane of the plate. The coordinate variables namely r, θ and z stand for the radial, circumferential and thickness directions, respectively.

The top surface $\left(z = h/2\right)$ of the plate is considered to be fully ceramic and the bottom surface $\left(\mathrm{z} = -h/2\right)$ to be fully metallic. The volume fractions of ceramics V_c and of metal V_m are taken to be of the form of a power function as

$$V_c\left(z\right) = \left(\frac{1}{2} + \frac{z}{h}\right)^k, \quad V_m = 1 - V_c \tag{1}$$

where, k denotes the power-law or volume fraction index. When the value of k is set to zero, the plate is ceramic-rich and when it tends to infinity, the plate becomes a metal-rich one. Therefore, according to the linear rule of mixtures, Young's modulus E and the mass density ρ can be obtained as follows

$$E(z)=(E_c-E_m)V_c(z)+E_m \tag{2-1}$$

$$\rho(z)=(\rho_c-\rho_m)V_c(z)+\rho_m, \tag{2-2}$$

where the subscripts m and c denote the metallic and ceramic phases, respectively. Poisson's ratio ν usually keep unchanged with the material constituents so, it is taken constant [2].

2.2. Governing equations of motion

Since the plate studied in this paper is considered to be thin, its thickness is small compared to the radius. Thus, the Kirchhoff plate theory is adequate to be used for describing the displacement field. u_1, u_2 and u_3 indicate the radial, circumferential and transvers displacements of any point inside the plate, respectively. According to this theory, the axisymmetric displacement components are expressed as

$$u_1=u(t,r)-z\frac{\partial w(t,r)}{\partial r},\qquad u_2=0,\qquad u_3=w(t,r). \tag{3}$$

where u and w represent the displacements at the mid-plane of the plate in the radial and thickness directions, respectively. Based on the von Kármán's assumption, the non-zero components of strain tensor are related to the displacement components as follows

$$\varepsilon_{11}=\varepsilon_{rr}=u_{1,r}+\frac{1}{2}(u_{3,r})^2,\qquad \varepsilon_{22}=\varepsilon_{\theta\theta}=\frac{1}{r}u_{2,\theta}+\frac{u_1}{r}. \tag{4}$$

where, the subscript comma symbols partial derivative. For a linear elastic material, the constitutive equation can be given by

$$\sigma_{ij}=\lambda\varepsilon_{kk}\delta_{ij}+2\mu\varepsilon_{ij}, \tag{5}$$

where, σ_{ij} indicates the classical stress tensor and the symbol δ denotes the Kronecker delta. The parameter λ and the shear modulus μ appeared in the preceding equation are referred to as the Lamé constants given by

$$\lambda=\frac{E\nu}{1-\nu^2},\qquad \mu=\frac{E}{2(1+\nu)}. \tag{6}$$

Using Eqs. (3) and (4), the strain-displacement relationships for the plate with moderately large axisymmetric deformations are given by

$$\varepsilon_{rr}=u_{,r}-zw_{,rr}+\frac{1}{2}w_{,r}^2,\qquad \varepsilon_{\theta\theta}=\frac{u}{r}-z\frac{w_{,r}}{r}. \tag{7}$$

The components of stress can be determined by introducing Eq. (7) into Eq. (5). The resultant forces and bending moments are then evaluated from the components of stress. Next, the elastic energies of the plate

and the work done by the external radial force applied to the FG plate, N_{r0}, are computed. Finally, applying the Hamilton's principle, the governing equations are obtained by

$$A_{11}\left(u_{,rr}+\frac{u_{,r}}{r}-\frac{u}{r^2}+w_{,r}w_{,rr}\right)-B_{11}\left(w_{,rrr}+\frac{w_{,rr}}{r}-\frac{w_{,r}}{r^2}\right)+\frac{A_{55}}{r}w_{,r}{}^2=I_1u_{,tt}-I_2w_{,rtt}, \tag{8-1}$$

$$\begin{aligned}&-D_{11}\nabla^4w+B_{11}\left(u_{,rrr}+\frac{2}{r}u_{,rr}-\frac{u_{,r}}{r^2}+\frac{u}{r^3}\right)+A_{11}\left(u_{,r}w_{,rr}+w_{,r}u_{,rr}+\frac{1}{2r}w_{,r}{}^3+\frac{3}{2}w_{,r}{}^2w_{,rr}\right)\\&+\left(\frac{A_{12}}{r}\right)\left(uw_{,rr}+2u_{,r}w_{,r}\right)+\left(\frac{B_{11}-3B_{12}}{r}\right)w_{,r}w_{,rr}+2\left(\frac{A_{55}}{r}\right)u_{,r}w_{,r}+\frac{1}{r}\frac{d}{dr}\left(r\,N_{r0}w_{,r}\right)\\&=I_1w_{,tt}+I_2\left(u_{,rtt}+\frac{1}{r}u_{,tt}\right)-I_3\left(w_{,rrtt}+\frac{1}{r}w_{,rtt}\right).\end{aligned} \tag{8-2}$$

where, $\nabla^4w=w_{,rrrr}+\frac{2}{r}w_{,rrr}-\frac{1}{r^2}w_{,rr}+\frac{1}{r^3}w_{,r}$. The stiffness coefficients and mass moments of inertia are expressed as

$$\{A_{11},B_{11},D_{11}\}=\int_{-\frac{h}{2}}^{\frac{h}{2}}\{\lambda(z)+2\mu(z)\}\{1,z,z^2\}dz,\ \{A_{12},B_{12}\}=\int_{-\frac{h}{2}}^{\frac{h}{2}}\lambda(z)\{1,z,z^2\}dz,\ 2A_{55}=(A_{11}-A_{12}) \tag{9-1}$$

$$\{I_1,I_2,I_3\}=\int_{-h/2}^{h/2}\rho(z)\{1,z,z^2\}dz \tag{9-2}$$

Further, the possible boundary conditions namely clamped and simply-supported ones are obtained as

Clamped edge:

$$u=w=w_{,r}=0 \qquad \text{at} \quad r = R \tag{10}$$

Simply-supported edge:

$$u=w=M_r=0 \qquad \text{at} \quad r = R \tag{11}$$

and the regular boundary condition at the center of the plate is

$$u=M_\theta-\left(rM_r\right)_{,r}-rN_rw_{,r}=w_{,r}=0 \qquad \text{at} \quad r = 0 \tag{12}$$

in which resultant force and moments are given by

$$N_r=A_{11}\left(u_{,r}+\frac{1}{2}w_{,r}^2\right)-B_{11}w_{,rr}+A_{12}\frac{u}{r}-B_{12}\frac{w_{,r}}{r}, \tag{13-1}$$

$$M_r=B_{11}\left(u_{,r}+\frac{1}{2}w_{,r}^2\right)-D_{11}w_{,rr}+B_{12}\frac{u}{r}-D_{12}\frac{w_{,r}}{r}, \tag{13-2}$$

$$M_\theta=B_{11}\frac{u}{r}-D_{11}\frac{w_{,r}}{r}+B_{12}\left(u_{,r}+\frac{1}{2}w_{,r}^2\right)-D_{12}w_{,rr}, \tag{13-3}$$

3. Numerical solution

There are various numerical techniques available for solving the nonlinear deferential equations under specific boundary conditions. Herein, the GDQ method is used to discretize and solve the governing equations under specific edge conditions. It is worth mentioning that, numerical methods suffer from time consumption particularly in complex problems including nonlinearities such as what we face in the current problem. Having said that, as compared to other numerical methods, the GDQ is an efficient method that converges rapidly to the final solution. Furthermore, as opposed to the finite element method, the GDQ is locking-free, does not require any assemblage process and is capable of satisfying both natural and essential boundary conditions. In the discretization, the solution domain is defined in $r_1 = -R < r < r_n = R$ and the mesh generation in the radial direction is taken as

$$r_i = R\left(\left(1-\cos\frac{i-1}{n-1}\pi\right)-1\right), \qquad i=1:n \tag{14}$$

where, n represents the number of discrete points.

3.1. Buckling problem

An important issue that need to be regarded is the effect of boundary conditions on the buckling behavior of the plates. Based on the previous publications [5, 33-36], the bifurcation buckling phenomenon does not occur for the unsymmetrical cross-ply laminated and FGM structures with at least one simply-supported or free edge. As elastic moduli of higher and lower surfaces of the structure are different for FGMs, curvature and moments are induced in the structures. For clamped FG structure, the induced moments are handled by the supports and the structure remains undeflected similar to homogeneous structures whereas, for simply-supported one, the bending moment is zero at the support and the structure starts to deflect at the onset of bending and buckling cannot exist. So, herein, the buckling and postbuckling phenomena are studied for clamped FG and simply-supported homogenous isotropic plates, only.

The beginning of the static instability of initial equilibrium state can be specified by solving the buckling problem leading to the determination of the critical buckling load. The problem is achieved by eliminating the time-dependent and nonlinear terms in Eqs. (8) and (13). So, applying the GDQ method, the discrete form of the linear counterpart of Eqs. (8) can be represented in a matrix format as follows

$$\mathbf{K}_L \begin{Bmatrix} \boldsymbol{u} \\ \boldsymbol{w} \end{Bmatrix} = -N_{r0}\mathbf{N}\begin{Bmatrix} \boldsymbol{u} \\ \boldsymbol{w} \end{Bmatrix} \tag{15}$$

where $\boldsymbol{u}$ and $\boldsymbol{w}$ are in the form of a column vector with n elements containing the nodal displacements. $\mathbf{K}_L$ and $\mathbf{N}$ stand for the conventional and geometric stiffness matrices, respectively with the size $2n \times 2n$ given by

$$\mathbf{K}_L = \begin{bmatrix} A_{11}\left(\mathbf{D}^{(2)} + \mathbf{r^d}\mathbf{D}^{(1)} - \left((\mathbf{r^d}) \circ^{\wedge} 2\right)\mathbf{I}\right) & -B_{11}\left(\mathbf{D}^{(3)} + \mathbf{r^d}\mathbf{D}^{(2)} - \left((\mathbf{r^d}) \circ^{\wedge} 2\right)\mathbf{D}^{(1)}\right) \\ B_{11}\left(\mathbf{D}^{(3)} + 2\mathbf{r^d}\mathbf{D}^{(2)} - \left((\mathbf{r^d}) \circ^{\wedge} 2\right)\mathbf{D}^{(1)} + \left((\mathbf{r^d}) \circ^{\wedge} 3\right)\mathbf{I}\right) & \boldsymbol{\Delta}^{(4)} \end{bmatrix} \tag{16-1}$$

$$\mathbf{N} = \begin{bmatrix} \mathbf{0} & \mathbf{0} \\ \mathbf{0} & \left(\mathbf{r^d}\mathbf{D}^{(1)} + \mathbf{D}^{(2)}\right) \end{bmatrix} \tag{16-2}$$

in which, $\boldsymbol{\Delta}^{(4)} = -D_{11}\left(\mathbf{D}^{(4)} + 2\mathbf{r^d}\mathbf{D}^{(3)} - \left((\mathbf{r^d}) \circ^{\wedge} 2\right)\mathbf{D}^{(2)} + \left((\mathbf{r^d}) \circ^{\wedge} 3\right)\mathbf{D}^{(1)}\right)$ and

$$\mathbf{r^d} = \begin{bmatrix} \frac{1}{r_1} & 0 & \cdots & 0 \\ 0 & \frac{1}{r_2} & \cdots & 0 \\ \vdots & \vdots & \ddots & \vdots \\ 0 & 0 & \cdots & \frac{1}{r_n} \end{bmatrix} \tag{17}$$

In Eq. (16-1), the symbol $\circ^{\wedge}$ represents the Hadamard product [13] to the power of a number i.e.,

$$\mathbf{x} \circ^{\wedge} n = \overbrace{\mathbf{x} \circ \mathbf{x} \circ \ldots \circ \mathbf{x}}^{n \text{ times}} \tag{18}$$

Also, $\mathbf{I}$ indicates an identity matrix with n^2 components and the differential operator $\mathbf{D}^{(m)}$ denotes the weighting coefficients matrix of the m[th]- order derivative in the GDQ method expressed as [37]

$$D_{ij}^{(m)} = \begin{cases} I_{ij} & m = 0 \\ \dfrac{\mathrm{P}\left(x_i\right)}{\left(x_i - x_j\right)\mathrm{P}\left(x_j\right)} & \text{where } \mathrm{P}\left(x_i\right) = \prod_{k=1;i\neq k}^{n}\left(x_i - x_k\right) \quad i, j = 1,\ldots n \text{ and } i \neq j \text{ and } m = 1 \\ r\left[D_{ij}^{(1)} D_{ii}^{(m-1)} - \dfrac{D_{ij}^{(m-1)}}{x_i - x_j}\right], & i \neq j \quad i, j = 1,\ldots,n \text{ and } m \geq 2 \\ -\sum_{\substack{k=1 \\ k\neq i}}^{n} D_{ik}^{(m)}, & i = j \quad i, j = 1,\ldots,n \text{ and } m \geq 2 \end{cases} \tag{19}$$

The related boundary conditions are transformed into the discrete form in a similar way. For example, for the simply-supported edge condition we get

$$\mathbf{u}_1 = \mathbf{u}_n = \mathbf{w}_1 = \mathbf{w}_n = \mathbf{M}_{\mathbf{r}}(1) = \mathbf{M}_{\mathbf{r}}(n) = 0 \tag{20}$$

where, $\mathbf{M}_{\mathbf{r}} = \left(B_{11}\mathbf{D}^{(1)} + B_{12}\mathbf{r}^{\mathbf{d}}\mathbf{I}\right)\mathbf{u} - \left(D_{11}\mathbf{D}^{(2)} + D_{12}\mathbf{r}^{\mathbf{d}}\mathbf{D}^{(1)}\right)\mathbf{w}$. After imposing the boundary conditions and making some manipulations, Eq. (15) is made into the standard form of an eigenvalue problem in the domain from which the critical buckling load can be determined.

3.2. Postbuckling problem

If the applied radial force exceeds the critical buckling load, the plate will lose its initial stability and will buckle [2]. To find the equilibrium path, the postbuckling configuration should be studied resulting from solving the nonlinear buckling problem. After dropping the time-dependent terms, the nonlinear governing equations given in Eqs. (8) are discretized by the GDQ method and can be stated in a condensed form as follows

$$\mathbf{K}_L \begin{Bmatrix} \boldsymbol{u}_s \\ \boldsymbol{w}_s \end{Bmatrix} + \begin{Bmatrix} \boldsymbol{Z}_1 \\ \boldsymbol{Z}_2 \end{Bmatrix} = 0 \tag{21}$$

where, the displacement variables in postbuckling region were denoted by $\boldsymbol{u}_s$ and $\boldsymbol{w}_s$, $\mathbf{K}_L$ has the same relationship as the one in the buckling analysis, Eq. (16-1), obtained by discretizing the linear terms in the governing equations. $\boldsymbol{Z}_1$ and $\boldsymbol{Z}_2$ are column vectors of *n* elements including the nonlinear terms given by

$$\boldsymbol{Z}_1 = A_{11}\left[\left(\mathbf{D}^{(1)}\mathbf{w}_\mathbf{s}\right)\circ\left(\mathbf{D}^{(2)}\mathbf{w}_\mathbf{s}\right)\right] + A_{55}\mathbf{ir}\circ\left((\mathbf{D}^{(1)}\mathbf{w}_\mathbf{s})\circ^{\wedge} 2\right) \tag{22-1}$$

$$\begin{aligned}\boldsymbol{Z}_2 = {} & A_{11}\left[\left(\mathbf{D}^{(1)}\mathbf{u}_\mathbf{s}\right)\circ\left(\mathbf{D}^{(2)}\mathbf{w}_\mathbf{s}\right) + \left(\mathbf{D}^{(2)}\mathbf{u}_\mathbf{s}\right)\circ\left(\mathbf{D}^{(1)}\mathbf{w}_\mathbf{s}\right) + \frac{1}{2}\mathbf{ir}\circ(\mathbf{D}^{(1)}\mathbf{w}_\mathbf{s})\circ^{\wedge} 3 + \frac{3}{2}(\mathbf{D}^{(2)}\mathbf{w}_\mathbf{s})\circ(\mathbf{D}^{(1)}\mathbf{w}_\mathbf{s})\circ^{\wedge} 2\right] + \\ & A_{12}\mathbf{ir}\circ\left[\mathbf{u}_\mathbf{s}\circ\left(\mathbf{D}^{(2)}\mathbf{w}_\mathbf{s}\right) + 2\left(\mathbf{D}^{(1)}\mathbf{u}_\mathbf{s}\right)\circ\left(\mathbf{D}^{(1)}\mathbf{w}_\mathbf{s}\right)\right] + \left(B_{11} - 3B_{12}\right)\mathbf{ir}\circ\left(\mathbf{D}^{(1)}\mathbf{w}_\mathbf{s}\right)\circ\left(\mathbf{D}^{(2)}\mathbf{w}_\mathbf{s}\right) + \\ & 2A_{55}\mathbf{ir}\circ\left(\mathbf{D}^{(1)}\mathbf{u}_\mathbf{s}\right)\circ\left(\mathbf{D}^{(1)}\mathbf{w}_\mathbf{s}\right) + \left[\mathbf{ir}\circ\left(\mathbf{D}^{(1)}\mathbf{w}_\mathbf{s}\right) + \left(\mathbf{D}^{(2)}\mathbf{w}_\mathbf{s}\right)\right]N_{r0} = 0\end{aligned} \tag{22-2}$$

in which, $\mathbf{ir} = \left[\frac{1}{r_1}, \frac{1}{r_2}, \cdots, \frac{1}{r_n}\right]^T$. Eq (21) includes $2n$ nonlinear equations of the form of

$$\begin{cases} \mathbf{F}\left(N_{r0}, \mathbf{u}_s, \mathbf{w}_s\right) = 0 \\ R^{2n+1} \to R^{2n} \end{cases} \tag{23}$$

This set of nonlinear equations along with the corresponding boundary conditions creates much difficulty to be solved by the linearization scheme. Hence, in the present paper, the aim is to solve the nonlinear problem through a direct solution approach which needs no linearization. This is achieved by adopting the Newton's method for which the initial values are taken as the solution of the linear problem associated with a specific mode obtained by eliminating the nonlinear terms in Eq. (21). For a special value of the radial force, however, this technique faces a challenge so that it gives the trivial solution when applied to the

nonlinear system of equations given in Eq. (23). To overcome this drawback and to attain the postbuckling path, a normalizing equation as a constraint is considered along with this system i.e.,

$$\begin{cases} \mathbf{F}\left(N_{r0}, \mathbf{u}_s, \mathbf{w}_s\right) = 0 \\ \mathbf{w}_s{}^T \mathbf{w}_s - c = 0 \end{cases} \tag{24}$$

where, c is the load controlling parameter that corresponds to the magnitude of buckling deformation. Now, solving the new system of equations by the Newton's method under the related boundary conditions traces the postbuckling path i.e., it achieves the applied radial force and the corresponding postbuckling configuration for a given value of the parameter c.

3.3. Free vibration of the prebuckled and postbuckled plate problem

To study the free vibration of the buckled plate, the variables of the displacement field are taken to be as the total of the buckled configuration and a small dynamic disturbance as [38]

$$u(r,t) = u_s(r) + d_u(r,t) \tag{25-1}$$

$$w(r,t) = w_s(r) + d_w(r,t) \tag{25-2}$$

where, d_u and d_w are the considered time-dependent disturbances around the buckled configuration taken to be of the form [38]

$$d_u(r,t) = \delta_u e^{i\omega t} \tag{26-1}$$

$$d_w(r,t) = \delta_w e^{i\omega t} \tag{26-2}$$

where ω is a natural frequency and δ_u, δ_w represent its corresponding mode shape. Substituting Eqs. (25)-(26) into Eqs. (8) and consequently, discretizing the resulting equations in a condensed form yield

$$\boldsymbol{K}_L \begin{Bmatrix} \boldsymbol{\delta}_\mathbf{u} \\ \boldsymbol{\delta}_\mathbf{w} \end{Bmatrix} + \begin{Bmatrix} \mathbf{G}_1 \\ \mathbf{G}_2 \end{Bmatrix} + \mathbf{F}\left(N_{r0}, \mathbf{u}_s, \mathbf{w}_s\right) = \omega^2 \mathbf{M}_\mathbf{L} \begin{Bmatrix} \boldsymbol{\delta}_\mathbf{u} \\ \boldsymbol{\delta}_\mathbf{w} \end{Bmatrix} \tag{27}$$

where, $\boldsymbol{\delta}_\mathbf{u}$ and $\boldsymbol{\delta}_\mathbf{w}$ are $n \times 1$ vectors and

$$\begin{aligned} \mathbf{G}_1 = A_{11}\Big[\left(\mathbf{D}^{(1)}\mathbf{w}_\mathbf{s}\right) \circ \left(\mathbf{D}^{(2)}\boldsymbol{\delta}_\mathbf{w}\right) + \left(\mathbf{D}^{(1)}\boldsymbol{\delta}_\mathbf{w}\right) \circ \left(\mathbf{D}^{(2)}\mathbf{w}_s\right) + \left(\mathbf{D}^{(1)}\boldsymbol{\delta}_\mathbf{w}\right) \circ \left(\mathbf{D}^{(2)}\boldsymbol{\delta}_\mathbf{w}\right)\Big] + \\ A_{55}\mathbf{ir} \circ \Big[\left(\mathbf{D}^{(1)}\boldsymbol{\delta}_\mathbf{w}\right) \circ^\wedge 2 + 2\left(\mathbf{D}^{(1)}\boldsymbol{\delta}_\mathbf{w}\right) \circ \left(\mathbf{D}^{(1)}\mathbf{w}_s\right)\Big] \end{aligned} \tag{28-1}$$

$$\mathbf{G}_2 = A_{11}[\left(\mathbf{D}^{(1)}\mathbf{u}_\mathbf{s}\right)\circ\left(\mathbf{D}^{(2)}\boldsymbol{\delta}_\mathbf{w}\right)+\left(\mathbf{D}^{(2)}\mathbf{w}_\mathbf{s}\right)\circ\left(\mathbf{D}^{(1)}\boldsymbol{\delta}_\mathbf{u}\right)+\left(\mathbf{D}^{(2)}\boldsymbol{\delta}_\mathbf{u}\right)\circ\left(\mathbf{D}^{(1)}\mathbf{w}_\mathbf{s}\right)+\left(\mathbf{D}^{(1)}\boldsymbol{\delta}_\mathbf{w}\right)\circ\left(\mathbf{D}^{(2)}\mathbf{u}_\mathbf{s}\right)+$$
$$\frac{3}{2}\mathbf{ir}\circ\left((\mathbf{D}^{(1)}\mathbf{w}_\mathbf{s})\circ\wedge 2\right)\circ\left(\mathbf{D}^{(1)}\boldsymbol{\delta}_\mathbf{w}\right)+\frac{3}{2}\left(\left((\mathbf{D}^{(1)}\mathbf{w}_\mathbf{s})\circ\wedge 2\right)\circ\left(\mathbf{D}^{(2)}\boldsymbol{\delta}_\mathbf{w}\right)+2\left(\mathbf{D}^{(1)}\mathbf{w}_\mathbf{s}\right)\circ\left(\mathbf{D}^{(1)}\boldsymbol{\delta}_\mathbf{w}\right)\circ\left(\mathbf{D}^{(2)}\mathbf{w}_\mathbf{s}\right)\right)+$$
$$\left(\mathbf{D}^{(1)}\boldsymbol{\delta}_\mathbf{u}\right)\circ\left(\mathbf{D}^{(2)}\boldsymbol{\delta}_\mathbf{w}\right)+\left(\mathbf{D}^{(2)}\boldsymbol{\delta}_\mathbf{u}\right)\circ\left(\mathbf{D}^{(1)}\boldsymbol{\delta}_\mathbf{w}\right)+\frac{1}{2}\mathbf{ir}\circ\left((\mathbf{D}^{(1)}\boldsymbol{\delta}_\mathbf{w})\circ\wedge 3+3\left((\mathbf{D}^{(1)}\boldsymbol{\delta}_\mathbf{w})\circ\wedge 2\right)\circ\left(\mathbf{D}^{(1)}\mathbf{w}_\mathbf{s}\right)\right)$$
$$+\frac{3}{2}\left(\left((\mathbf{D}^{(1)}\boldsymbol{\delta}_\mathbf{w})\circ\wedge 2\right)\circ\left(\mathbf{D}^{(2)}\mathbf{w}_\mathbf{s}\right)+\left((\mathbf{D}^{(1)}\boldsymbol{\delta}_\mathbf{w})\circ\wedge 2\right)\circ\left(\mathbf{D}^{(2)}\boldsymbol{\delta}_\mathbf{w}\right)\right)+3\left(\mathbf{D}^{(1)}\mathbf{w}_\mathbf{s}\right)\circ\left(\mathbf{D}^{(1)}\boldsymbol{\delta}_\mathbf{w}\right)\circ\left(\mathbf{D}^{(2)}\boldsymbol{\delta}_\mathbf{w}\right)]+ \tag{28-2}$$
$$A_{12}\mathbf{ir}\circ[\mathbf{u}_\mathbf{s}\circ\left(\mathbf{D}^{(2)}\boldsymbol{\delta}_\mathbf{w}\right)+\boldsymbol{\delta}_\mathbf{u}\circ\left(\mathbf{D}^{(2)}\mathbf{w}_\mathbf{s}\right)+2\left(\mathbf{D}^{(1)}\mathbf{u}_\mathbf{s}\right)\circ\left(\mathbf{D}^{(1)}\boldsymbol{\delta}_\mathbf{w}\right)+2\left(\mathbf{D}^{(1)}\mathbf{w}_\mathbf{s}\right)\circ\left(\mathbf{D}^{(1)}\boldsymbol{\delta}_\mathbf{w}\right)+$$
$$\boldsymbol{\delta}_\mathbf{u}\circ\left(\mathbf{D}^{(2)}\boldsymbol{\delta}_\mathbf{w}\right)+2\left(\mathbf{D}^{(1)}\boldsymbol{\delta}_\mathbf{u}\right)\circ\left(\mathbf{D}^{(1)}\boldsymbol{\delta}_\mathbf{w}\right)]+\left(B_{11}-3B_{12}\right)\mathbf{ir}\circ[\left(\mathbf{D}^{(1)}\mathbf{w}_\mathbf{s}\right)\circ\left(\mathbf{D}^{(2)}\boldsymbol{\delta}_\mathbf{w}\right)+\left(\mathbf{D}^{(2)}\mathbf{w}_\mathbf{s}\right)\circ\left(\mathbf{D}^{(1)}\boldsymbol{\delta}_\mathbf{w}\right)+$$
$$\left(\mathbf{D}^{(1)}\boldsymbol{\delta}_\mathbf{w}\right)\circ\left(\mathbf{D}^{(2)}\boldsymbol{\delta}_\mathbf{w}\right)]+2A_{55}\mathbf{ir}\circ[\left(\mathbf{D}^{(1)}\mathbf{u}_\mathbf{s}\right)\circ\left(\mathbf{D}^{(1)}\boldsymbol{\delta}_\mathbf{w}\right)+\left(\mathbf{D}^{(1)}\boldsymbol{\delta}_\mathbf{u}\right)\circ\left(\mathbf{D}^{(1)}\mathbf{w}_\mathbf{s}\right)+\left(\mathbf{D}^{(1)}\boldsymbol{\delta}_\mathbf{u}\right)\circ\left(\mathbf{D}^{(1)}\boldsymbol{\delta}_\mathbf{w}\right)]+$$
$$[\mathbf{ir}\circ\left(\mathbf{D}^{(1)}\boldsymbol{\delta}_\mathbf{w}\right)+\left(\mathbf{D}^{(2)}\boldsymbol{\delta}_\mathbf{w}\right)]N_{r0}$$

$$\mathbf{M}_\mathbf{L}=\begin{bmatrix}-I_1\mathbf{I} & I_2\mathbf{D}^{(1)}\\ -I_2\left(\mathbf{r}^\mathbf{d}\mathbf{I}+\mathbf{D}^{(1)}\right) & -I_1\mathbf{I}+I_3\left(\mathbf{D}^{(2)}+\mathbf{r}^\mathbf{d}\mathbf{D}^{(1)}\right)\end{bmatrix} \tag{28-3}$$

Since the dynamic disturbances are assumed to be small in comparison with the postbuckling configuration, one can get the linear free vibration problem by dropping the nonlinear terms from Eq. (27) [38]. By introducing matrices $\bar{\mathbf{u}}_\mathbf{s}$ and $\bar{\mathbf{w}}_\mathbf{s}$ as

$$\bar{\mathbf{u}}_\mathbf{s}=\mathbf{u}_\mathbf{s}\begin{bmatrix}1 & 1 & \cdots & 1\end{bmatrix}_{1\times n},\ \bar{\mathbf{w}}_\mathbf{s}=\mathbf{w}_\mathbf{s}\begin{bmatrix}1 & 1 & \cdots & 1\end{bmatrix}_{1\times n} \tag{29}$$

and regarding $\mathbf{F}\left(N_{r0},\mathbf{u}_s,\mathbf{w}_s\right)=0$, Eq. (27) then becomes

$$\left(\boldsymbol{K}_\mathbf{L}+\begin{bmatrix}\mathbf{K}_{11}^* & \mathbf{K}_{12}^*\\ \mathbf{K}_{21}^* & \mathbf{K}_{22}^*\end{bmatrix}\right)\begin{Bmatrix}\boldsymbol{\delta}_\mathbf{u}\\ \boldsymbol{\delta}_\mathbf{w}\end{Bmatrix}=\omega^2\mathbf{M}_\mathbf{L}\begin{Bmatrix}\boldsymbol{\delta}_\mathbf{u}\\ \boldsymbol{\delta}_\mathbf{w}\end{Bmatrix} \tag{30}$$

in which,

$$\mathbf{K}_{11}^*=\mathbf{0},\qquad \mathbf{K}_{12}^*=A_{11}\left[\left(\mathbf{D}^{(1)}\bar{\mathbf{w}}_\mathbf{s}\right)\circ\mathbf{D}^{(2)}+\left(\mathbf{D}^{(2)}\bar{\mathbf{w}}_\mathbf{s}\right)\circ\mathbf{D}^{(1)}\right]+2A_{55}\mathbf{r}^\mathbf{d}\left[\left(\mathbf{D}^{(1)}\bar{\mathbf{w}}_\mathbf{s}\right)\circ\mathbf{D}^{(1)}\right] \tag{31-1}$$

$$\mathbf{K}_{21}^*=A_{11}\left[\left(\mathbf{D}^{(1)}\bar{\mathbf{w}}_\mathbf{s}\right)\circ\mathbf{D}^{(2)}+\left(\mathbf{D}^{(2)}\bar{\mathbf{w}}_\mathbf{s}\right)\circ\mathbf{D}^{(1)}\right]+A_{12}\mathbf{r}^\mathbf{d}\left[\left(\mathbf{D}^{(2)}\bar{\mathbf{w}}_\mathbf{s}\right)\circ\mathbf{I}+2\left(\mathbf{D}^{(1)}\bar{\mathbf{w}}_\mathbf{s}\right)\circ\mathbf{D}^{(1)}\right]+$$
$$2A_{55}\mathbf{r}^\mathbf{d}\left[\left(\mathbf{D}^{(1)}\bar{\mathbf{w}}_\mathbf{s}\right)\circ\mathbf{D}^{(1)}\right] \tag{31-2}$$

$$\mathbf{K}_{22}^*=A_{11}[\left(\mathbf{D}^{(1)}\bar{\mathbf{u}}_\mathbf{s}\right)\circ\mathbf{D}^{(2)}+\left(\mathbf{D}^{(2)}\bar{\mathbf{u}}_\mathbf{s}\right)\circ\mathbf{D}^{(1)}+\frac{3}{2}\mathbf{r}^\mathbf{d}\left(\left((\mathbf{D}^{(1)}\bar{\mathbf{w}}_\mathbf{s})\circ\wedge 2\right)\circ\mathbf{D}^{(1)}\right)+\frac{3}{2}\left((\mathbf{D}^{(1)}\bar{\mathbf{w}}_\mathbf{s})\circ\wedge 2\right)\circ\mathbf{D}^{(2)}$$
$$+3\left(\left(\mathbf{D}^{(1)}\bar{\mathbf{w}}_\mathbf{s}\right)\circ\left(\mathbf{D}^{(2)}\bar{\mathbf{w}}_\mathbf{s}\right)\right)\circ\mathbf{D}^{(1)}]+A_{12}\mathbf{r}^\mathbf{d}\left[\bar{\mathbf{u}}_\mathbf{s}\circ\mathbf{D}^{(2)}+2\left(\mathbf{D}^{(1)}\bar{\mathbf{u}}_\mathbf{s}\right)\circ\mathbf{D}^{(1)}\right]+2A_{55}\mathbf{r}^\mathbf{d}\left[\left(\mathbf{D}^{(1)}\bar{\mathbf{u}}_\mathbf{s}\right)\circ\mathbf{D}^{(1)}\right]+ \tag{31-3}$$
$$\left(B_{11}-3B_{12}\right)\mathbf{r}^\mathbf{d}\left[\left(\mathbf{D}^{(1)}\bar{\mathbf{w}}_\mathbf{s}\right)\circ\mathbf{D}^{(2)}+\left(\mathbf{D}^{(2)}\bar{\mathbf{w}}_\mathbf{s}\right)\circ\mathbf{D}^{(1)}\right]+\left(\mathbf{r}^\mathbf{d}\mathbf{D}^{(1)}+\mathbf{D}^{(2)}\right)N_{r0}$$

Substituting the boundary conditions into Eq. (30) and separating the domain and boundary grid points, assigned by the subscripts **d** and **b**, respectively, from each other by defining the vectors $\mathbf{X_d} = \left\{ (\boldsymbol{\delta_u})_{\mathbf{d}}^{\boldsymbol{T}} , (\boldsymbol{\delta_w})_{\mathbf{d}}^{\boldsymbol{T}} \right\}^{\mathrm{T}}$, $\mathbf{X_b} = \left\{ (\boldsymbol{\delta_u})_{\mathbf{b}}^{\boldsymbol{T}} , (\boldsymbol{\delta_w})_{\mathbf{b}}^{\boldsymbol{T}} \right\}^{\mathrm{T}}$, this equation can be rewritten as

$$\begin{bmatrix} \mathbf{K_{dd}} & \mathbf{K_{db}} \\ \mathbf{K_{bd}} & \mathbf{K_{bb}} \end{bmatrix} \begin{Bmatrix} \mathbf{X_d} \\ \mathbf{X_b} \end{Bmatrix} = \omega^2 \begin{bmatrix} \mathbf{M_{dd}} & \mathbf{M_{db}} \\ 0 & 0 \end{bmatrix} \begin{Bmatrix} \mathbf{X_d} \\ \mathbf{X_b} \end{Bmatrix} \tag{32}$$

From the preceding equation an eigenvalue problem in the domain is extracted as

$$\left(\mathbf{K_{dd}} - \mathbf{K_{db}} \mathbf{K_{bb}}^{-1} \mathbf{K_{bd}} \right) \mathbf{X_d} = \omega^2 \left(\mathbf{M_{dd}} - \mathbf{M_{db}} \mathbf{K_{bb}}^{-1} \mathbf{K_{bd}} \right) \mathbf{X_d} \tag{33}$$

Using Eq. (33), one can obtain the vibrations natural frequencies of the plate for any given radial load around the corresponding buckled configuration.

In the case of prebuckling problem, by taking the value of the applied load in the domain $0 \le N_{r0} \le P_{crit}$, where P_{crit} denotes the critical buckling load for a given mode, and setting the variables of displacement in postbuckling $\bar{\mathbf{u}}_{\mathbf{s}}$ and $\bar{\mathbf{w}}_{\mathbf{s}}$ to zero, the natural frequencies of the plate around the initial undeflected position are determined.

4. Results and discussion

In the following, the results obtained by the solution of the buckling, postbuckling and free vibrations of the undeflected and buckled FG plate are presented and compared for fully-clamped and simply-supported edge supports. The FG plate is considered to be made of aluminum and alumina, respectively with the material properties as [2]

Metal: $E_m = 70\,GPa,\ \ \rho_m = 2707 \dfrac{kg}{m^3}$

Ceramic: $E_c = 380\,GPa,\ \ \rho_c = 3800 \dfrac{kg}{m^3}$

unless otherwise specified. Moreover, Poisson's ratio is selected to be constant as 0.3 [2].

In the numerical computations, the following non-dimensional parameters are evaluated

Central deflection ratio = $\dfrac{w_{\max}}{h}$

Non-dimensional radial load = $\dfrac{N_{r0} R^2}{E_m h^3}$

Non-dimensional natural frequency = $\dfrac{\omega R^2}{h} \sqrt{12 \rho_m \left(1 - \nu^2\right) / E_m}$

where $w_{\max}$ denotes the maximum deflection of the plate; other parameters were all defined in the previous sections. Also, the aspect ratio (h/R) is considered to be 0.04, unless otherwise specified.

It is first necessary to make certain that the present results converge, so the convergence of the numerical solution proposed herein is examined. Fig. 2 represents the central deflection ratio of the clamped FG circular plate corresponding to the first buckled configuration against non-dimensional radial load for a numbers of grid points. The volume fraction index is taken to be $k=3$. As depicted, by increasing the number of grid point, the gap between the curves diminishes so that it perfectly disappears when n reaches 22. Thus, $n=22$ is chosen as the appropriate number of grid point in all the numerical computations. Also, numerical simulations show that the linear results such as the critical buckling load and the natural frequency rapidly converge setting $n=14$. This study verifies the fast convergence of the present numerical method.

To verify the accuracy of the presented numerical model, several comparison examples are given. In the first example, the critical buckling loads of clamped circular FG plates are calculated for a number of volume fractions and the ratios h/R and compared with those of Ref. [2] based on the classical plate theory (CPT) and first-order shear deformation theory (FSDT) in Table 1. The results agree well with each other.

In the second example, the first four non-dimensional linear natural frequencies of clamped FG circular plates for axisymmetric vibrations are compared with those of Ref. [3] in Table 2. The results are provided for different values of volume fraction and the aspect ratio $h/R=0.04$. Herein, the metal and ceramics phases of FGM system are assumed to be stainless steel and silicon nitride, respectively. Material properties are also dependent on temperature according to Ref. [3]. As observed, the two sets of results are in a good agreement. It is obvious in the previous tables that as the volume fraction index is increased, the critical buckling load and the natural frequency are decreased. It is because that the increase of volume fraction index causes the stiffness of the plate to decrease.

As the third example, postbuckling behavior of clamped FG circular plates predicted by the present study is compared with the one by Ref. [5] based on the FSDT in Fig. 3. The results are generated for the FG material system of aluminum–zirconia taken in Ref. [5] based on which setting $k=0$ and $k=\infty$ result in a fully metallic and fully ceramic plate, respectively. It is also assumed that $h/R=0.02$. It is observed from this figure that the two curves are quite close to each other specifically at small non-dimensional loads. The starting points of the postbuckling paths corresponding to the critical buckling load almost coincide. However, at higher loads, there is a small gap (maximum 5.5%) between the two responses which may be due to the different theories used.

In what follows, the influences of material model parameters and edge conditions on postbuckling and free vibrations behavior of the undeflected and buckled functionally graded plate are examined. As discussed in

section 3-1, the clamped FG plates behave like homogenous isotropic plates and buckling occurs for them while, the FG plates with at least one simply-supported or free edge start to bend when subjected to in-plane compressive loading. Since the present work focuses on the vibrations of the circular plates around the prebuckling and postbuckling configurations, the response of FG clamped and homogenous isotropic simply-supported plates is evaluated, only. Accordingly, the results are provided for different volume fraction indices when the plate is all edges clamped and for $k = 0$ and $k = \infty$, i.e., rich-ceramic and rich-metal plates, when it is all edges simply-supported.

The central deflection ratio of the circular plate for the first buckled configuration versus non-dimensional radial load is depicted in Fig. 4. It is observed from this figure that when the non-dimensional radial load passes the bifurcation point (i.e., the critical buckling load), the plate loses the straight configuration and gains a new stable equilibrium position namely postbuckling configuration. It is obvious that increasing the radial load causes the central deflection ratio to rise. Furthermore, one can see that the ceramic- and the metal-rich plates have the minimum and maximum deflection and so, the stiffest and the most flexible flexural behavior in the postbuckling region, respectively.

Presented in Fig. 5 is the postbuckling behavior of clamped and simply-supported homogenous circular plates corresponding to the first buckled mode. From this figure, it is seen that the starting points of the curves associated with clamped plate are at larger radial force (i.e., larger critical buckling load) as compared to simply supported plate. Moreover, for a specific value of radial force, the central deflection ratio of the plate with clamped edge conditions is lower than that of the plate with simply-supported end conditions. In other words, the plate with stiffer edge supports has higher strength against the load. It is noticeable that the curves corresponding to the two edge conditions converge, as the non-dimensional radial load is increased. It means that at higher loads, the effect of edge conditions on deflection of the plate in the postbuckling region gets nullified.

Variation of the non-dimensional fundamental natural frequency of the circular plate around prebuckled configuration with non-dimensional radial load is indicated in Fig. 6. The starting points of the curves correspond to the linear fundamental natural frequency. As shown, for all the materials considered, the natural frequency of the plate diminishes with the increase of the non-dimensional radial load so that it tends to zero when the load approaches its critical value. In other words, applying the radial force as much as the critical buckling load makes the undeflected configuration unstable. It is also found from Fig. 6 (a) that for the plate with smaller volume fraction indices, stability of the straight position lasts longer compared to the one with higher indices due to having the greater critical buckling load.

Fig. 7 shows the first natural frequency of the circular plate around the initial position and the first postbuckled configuration against the radial load. It is observed that, increasing the radial load beyond the critical buckling load causes the first natural frequency to increase. In other words, it is found that trend in

variations of the fundamental natural frequency with the applied radial load around the prebuckled configuration differs from the one around the buckled configuration, as shown in Fig. 7. Moreover, it is interesting to note that in the postbuckling region, the natural frequency of the rich-metal structure is larger than that of the rich-ceramic structure which is in contrast to the result obtained in the prebuckling region. For the selected material properties, the mass density of the metal is smaller than that of the ceramics. Therefore, it can be concluded that in the postbuckling region, the effect of inertia dominates the effect of stiffness.

To address this issue further, an FG material system of stainless steel–silicon nitride is selected for which the mass density of the metal is larger than that of the ceramics ($E_m = 201.04\,GPa,\ E_c = 348.43\,GPa,\ \rho_m = 8166\ kg/m^3,\ \rho_c = 2370\,kg/m^3$). The free vibrations behavior of the circular plate made of this material around the postbuckling configuration is shown in Fig. 8. It is observed that like the prebuckling region, the maximum and minimum natural frequencies are obtained for ceramic- and metal-rich plates, respectively.

It is worth mentioning that the first buckled configuration is a stable equilibrium position [38]. Also, the first natural frequency is of more significance in comparison to the higher modes so, herein, the natural frequency of FG circular plate related to the lowest vibration mode around the first buckled configuration is evaluated. Moreover, the model developed in the present work is axisymmetric that for its antiaxisymmetric counterpart, the natural frequencies corresponding to the higher modes are less important.

5. Conclusion

In this work, the buckling, postbuckling and vibrations around the buckled configuration behaviors of the functionally graded circular plate were investigated. The nonlinear governing equations of motion together with the related boundary conditions were extracted based on the Kirchhoff plate theory and solved by the generalized differential quadrature method. Through several comparative studies, the reliability of the present model was assessed. It was shown that the present method has a high rate convergence and accuracy. The first natural frequency when no load is applied and the critical buckling load of the plate were obtained and it was found that the clamped plate has higher value of these parameters than the simply-supported one. It was shown that the lower value of volume fraction index, the higher critical buckling load and the first natural frequency as well as the stiffer flexural behavior in the postbuckling region. Further, it was observed that as the radial force is increased, the effect of edge supports on deflection of the plate in the postbuckling region becomes less pronounced. It was also discerned that as the radial load is increased, the fundamental natural frequency of the plate around the prebuckled position is decreased, whereas it is increased around the first buckled configuration. The present work showed that the inertia and stiffness may play different

role in vibrations of plates with different equilibrium positions. More clearly, in the postbuckling configuration, it was found that the effect of inertia is dominant (in contrast to the prebuckling region) so that the material with smaller mass density has higher natural frequency than the one with higher elastic modulus. So, one can find the importance of the knowledge of the vibrational behavior of the plates at different equilibrium positions in design process, as the structures may behave quite different when they vibrates around the prebuckled or postbuckled configuration.

6. Funding

This research received no specific grant from any funding agency in the public, commercial, or not-for-profit sectors.

7. Declaration of conflicting interests

The authors declare that there is no actual or potential conflict of interest that could influence our work.

8. Acknowledgments

The authors thank the Stam Sanat Company (a member of Ezam Automotive Parts Group) for their support.

References

1. Sofiyev, A.H. "The vibration and stability behavior of freely supported FGM conical shells subjected to external pressure", *Composite Structures*, **89**(3), pp. 356-366 (2009).

2. Najafizadeh, M.M., and Hedayati, B. "Refined theory for thermoelastic stability of functionally graded circular plates", *Journal of Thermal Stresses*, **27**(9), pp. 857-880 (2004).

3. Allahverdizadeh, A., Naei, M.H., and Nikkhah Bahrami, M. "Nonlinear free and forced vibration analysis of thin circular functionally graded plates", *Journal of Sound and Vibration*, **310**(4-5), pp. 966-984 (2008).

4. Sepahi, O., Forouzan, M.R., and Malekzadeh, P. "Thermal buckling and postbuckling analysis of functionally graded annular plates with temperature-dependent material properties", *Materials Design*, **32**(7), pp. 4030-4041 (2011).

5. Fallah, F., Vahidipoor, M.K., and Nosier, A. "Post-buckling behavior of functionally graded circular plates under asymmetric transverse and in-plane loadings", *Composite Structures*, **125**, pp. 477-488 (2015).

6. Ansari, R., Shahabodini, A., and Shojaei, M.F. "Vibrational analysis of carbon nanotube-reinforced composite quadrilateral plates subjected to thermal environments using a weak formulation of elasticity", *Composite Structures*, **139**, pp. 167-187 (2016).

7. Żur, K.K. "Green's function in frequency analysis of circular thin plates of variable thickness", *Journal of Theoretical and Applied Mechanics*, **53**(4), pp. 873-884 (2015).

8. Żur, K.K. "Green's function for frequency analysis of thin annular plates with nonlinear variable thickness", *Applied Mathematical Modelling*, **40** (5-6), pp. 3601-3619 (2016).

9. Żur, K.K. "Green's function approach to frequency analysis of thin circular plates", *Bulletin of the Polish Academy of Sciences. Technical Sciences*, **64**(1), (2016).

10. Żur, K.K. "Free vibration analysis of elastically supported functionally graded annular plates via quasi-Green's function method", *Composites Part B: Engineering,* **144**, pp. 37-55 (2018).

11. Żur, K.K. "Multiparametric analytical solution for the eigenvalue problem of FGM porous circular plates", *Symmetry*, **11**(3), p. 429 (2019).

12. Shahabodini, A., Gholami, Y., Ansari, R., et al. "Vibration analysis of graphene sheets resting on Winkler/Pasternak foundation: A multiscale approach", *The European Physical Journal Plus*, **134**(10), pp. 1-15 (2019).

13. Gholami, Y., Shahabodini, A., Ansari, R., et al. "Nonlinear vibration analysis of graphene sheets resting on Winkler–Pasternak elastic foundation using an atomistic-continuum multiscale model", *Acta Mech*anica, **230**(12), pp. 4157-4174 (2019).

14. Nikbakht, S., Kamarian, S., and Shakeri, M. "A review on optimization of composite structures Part II: Functionally graded materials", *Composite Struct*ures, 214, pp. 83-102 (2019).

15. Smita, P., and Mohanty, S.C. "Nonlinear free vibration analysis of functionally graded plate resting on elastic foundation in thermal environment using higher-order shear deformation theory", *Scientia Iranica*, **26**(2), pp. 815-833 (2019).

16. Gholami, R., and Ansari, R. "On the vibration of postbuckled functionally graded-carbon nanotube reinforced composite annular plates", *Scientia Iranica*, **26**(2), pp. 3857-3874 (2019).

17. Atri, H.R., and Shojaee, S. "Analysis of laminated composite plates based on THB-RKPM method using the higher order shear deformation plate theory", *Scientia Iranica*, **26**(4), pp. 2057-2078 (2019).

18. Li, M., Soares, C.G., and Yan, R. "A novel shear deformation theory for static analysis of functionally graded plates", *Composite Structures*, **250**, p. 112559 (2020).

19. Sharma, T.K. "Free vibration analysis of functionally graded circular piezoelectric plate using COMSOL multiphysics", *In AIP Conference Proceedings*, AIP Publishing LLC, 2220(1), p. 080017 (2020).

20. Radaković, A., Čukanović, D., Bogdanović, G., et al. "Thermal buckling and free vibration analysis of functionally graded plate resting on an elastic foundation according to high order shear deformation theory based on new shape function", *Applied Sci*ences, **10**(12), p. 4190 (2020).

21. Lal, R., and Saini, R. "Vibration analysis of functionally graded circular plates of variable thickness under thermal environment by generalized differential quadrature method", *Journal of Vibration and Control*, **26**(1-2), pp. 73-87 (2020).

22. Xu, P., and Wellens, P. "Effects of static loads on the nonlinear vibration of circular plates", *Journal of Sound and Vibration*, **504**, p. 116111 (2021).

23. Imran, M., Khan, R., and Badshah, S. "Experimental, analytical, and finite element vibration analyses of delaminated composite plates", *Scientia Iranica*, **28**(1), pp. 231-240 (2021).

24. Qin, X., Shen, Y., Chen, W., et al. "Bending and free vibration analyses of circular stiffened plates using the FSDT mesh-free method", *International Journal of Mechanical Sciences*, **202**, p. 106498 (2021).

25. Javani, M., Kiani, Y., and Eslami, M.R. "Geometrically nonlinear free vibration of FG-GPLRC circular plate on the nonlinear elastic foundation", *Composite Structures*, **261**, p. 113515 (2021).

26. Sobhy, M. "3-D elasticity numerical solution for magneto-hygrothermal bending of FG graphene/metal circular and annular plates on an elastic medium", *European Journal of Mechanics-A/Solids*, **88**, p. 104265 (2021).

27. Hilali, Y., and Bourihane, O. "A mixed MLS and Hermite-type MLS method for buckling and postbuckling analysis of thin plates", *Structures*, **33**, pp. 2349-2360 (2021).

28. Singh, S.D., and Sahoo, R. "Analytical solution for static and free vibration analysis of functionally graded CNT-reinforced sandwich plates", *Archive of Applied Mechanics*, pp. 1-16 (2021).

29. Singh, V., Kumar, R., and Patel, S.N. "Parametric instability analysis of functionally graded CNT-reinforced composite (FG-CNTRC) plate subjected to different types of non-uniform in-plane loading", *Emerging Trends of Advanced Composite Materials in Structural Applications*, pp. 291-312 (2021).

30. Sladek, J., Sladek, V., Krahulec, S., et al. "Analyses of circular magnetoelectroelastic plates with functionally graded material properties", *Mechanics of Advanced Materials and Structures,* **22**(6), pp. 479-489 (2015).

31. Saadatmand, M., and Kook, J. "Multi-objective optimization of a circular dual back-plate MEMS microphone: tradeoff between pull-in voltage, sensitivity and resonance frequency", *Microsystem Technologies*, **25**(8), pp. 2937-2947 (2019).

32. Ansari, R., Faghih Shojaei, M., Mohammadi, V., et al. "Size-dependent vibrations of post-buckled functionally graded Mindlin rectangular microplates", *Latin American Journal of Solids and Structures*, **11**, pp. 2351-2378 (2014).

33. Leissa, A.W. "Conditions for laminated plates to remain flat under inplane loading", *Composite Structures*, **6**(4), pp. 261-270 (1986).

34. Hui-Shen, S. "Thermal postbuckling behavior of shear deformable FGM plates with temperature-dependent properties", *International Journal of Mechanical Sciences*, **49**(4), pp. 466-478 (2007).

35. Hui-Shen S. "Nonlinear bending response of functionally graded plates subjected to transverse loads and in thermal environments", *International Journal of Mechanical Sciences*, **44**(3), pp. 561-584 (2002).

36. Piotr, J., Żur, K.K., Kim, J., et al. "On the bifurcation buckling and vibration of porous nanobeams", *Composite Structures,* **250**, p. 112632 (2020).

37. Shu, C. "Differential quadrature and its application in engineering", Springer Science & Business Media (2000).

38. Nayfeh, A.H, and Emam, S.A. "Exact solution and stability of postbuckling configurations of beams", *Nonlinear Dyn*amics, **54**(4), pp. 395-408 (2008).

List of captions

1. Figure 1: Schematic of a functionally graded circular plate, geometric parameters and coordinate system
2. Figure 2: Convergence of the postbuckling path of the clamped functionally graded circular plate for the first buckled configuration
3. Figure 3: Comparison of the postbuckling paths of the clamped functionally graded circular plate for the first buckled configuration

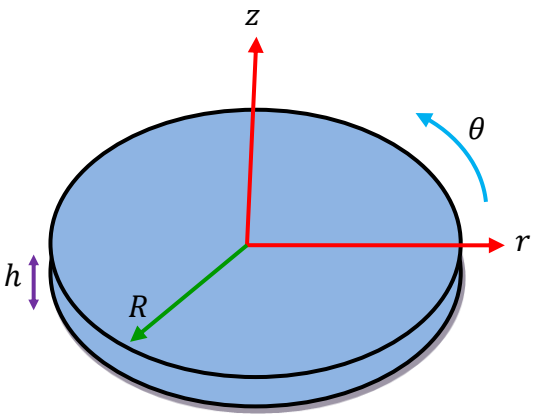

Fig. 1: Schematic of a functionally graded circular plate, geometric parameters and coordinate system

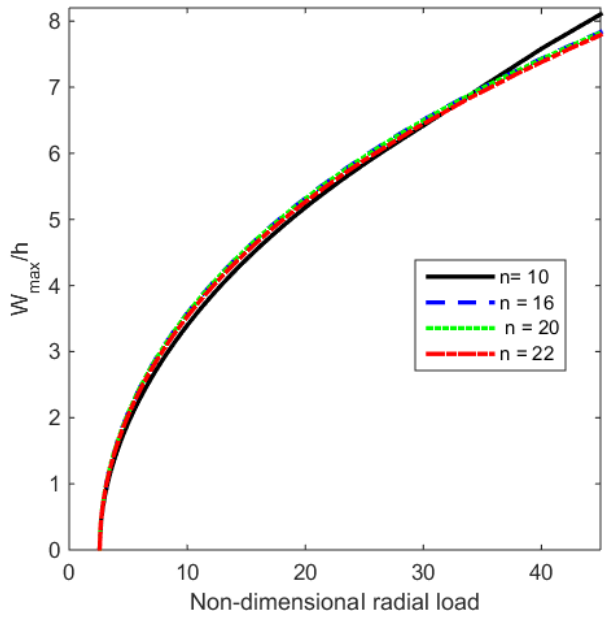

Fig. 2: Convergence of the postbuckling path of the clamped functionally graded circular plate for the first buckled configuration

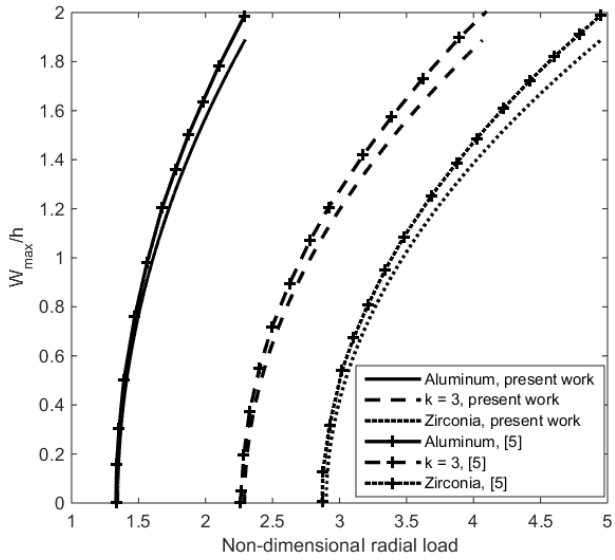

Fig. 3: Comparison of the postbuckling paths of the clamped functionally graded circular plate for the first buckled configuration

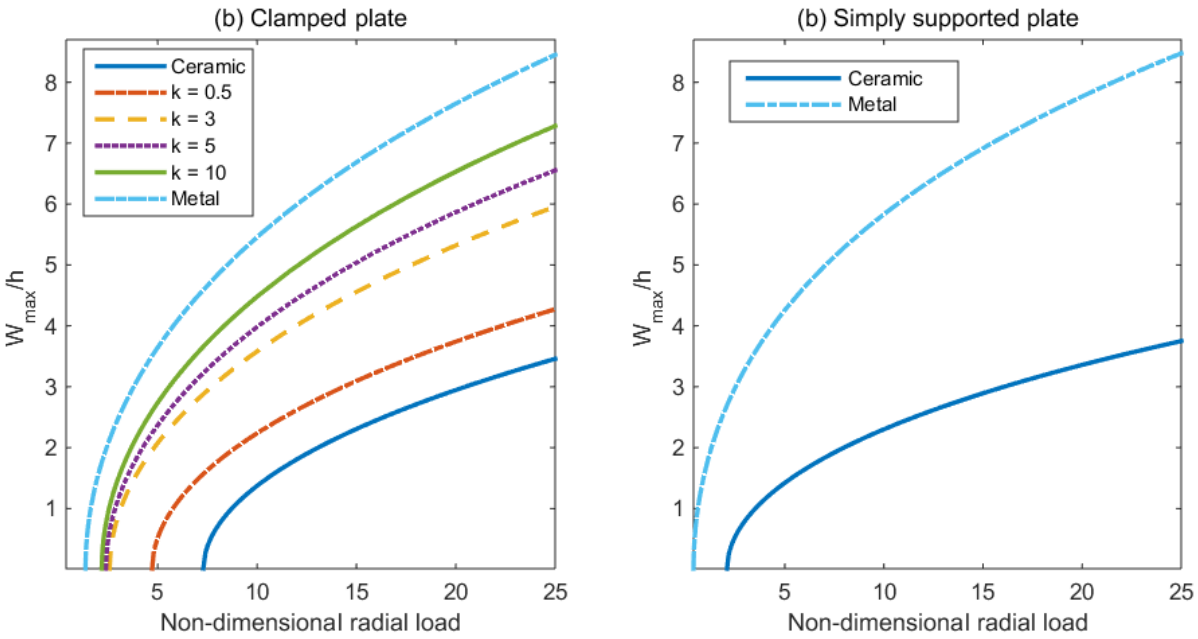

Fig. 4: Static bifurcation diagrams of the circular plate for the first buckled configuration

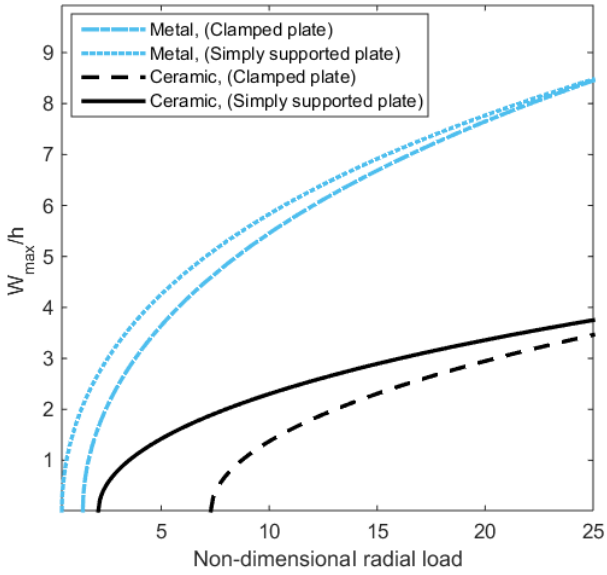

Fig. 5: Postbuckling behavior of the homogenous circular plate with clamped and simply-supported edge conditions for the first buckled configuration

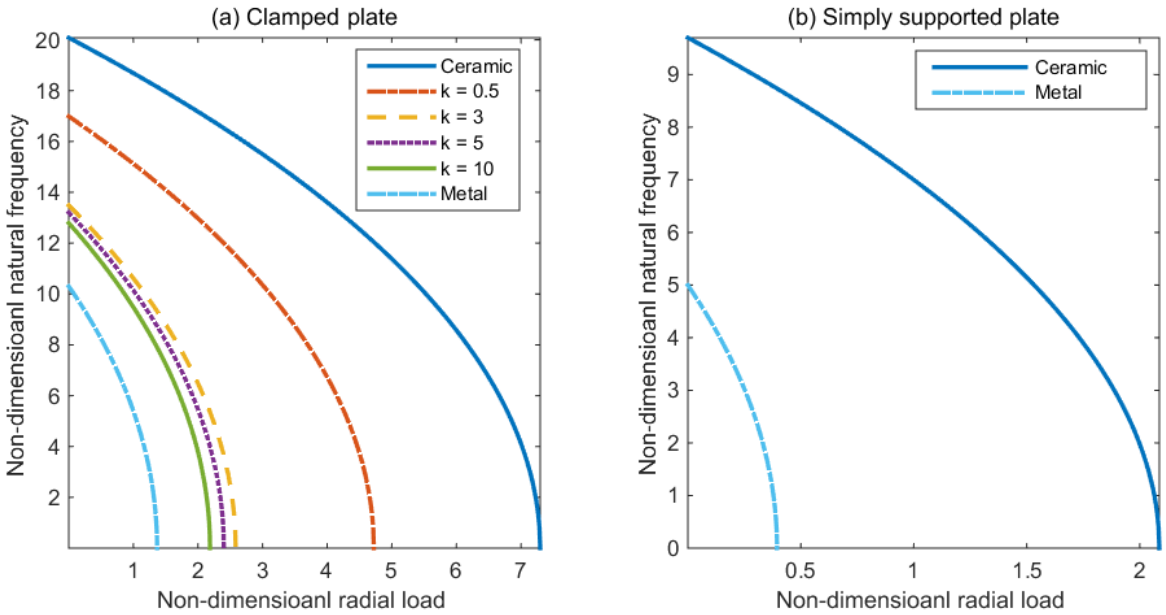

Fig. 6: Non-dimensional first natural frequency of the circular plate around the initial undeflected configuration versus non-dimensional radial load

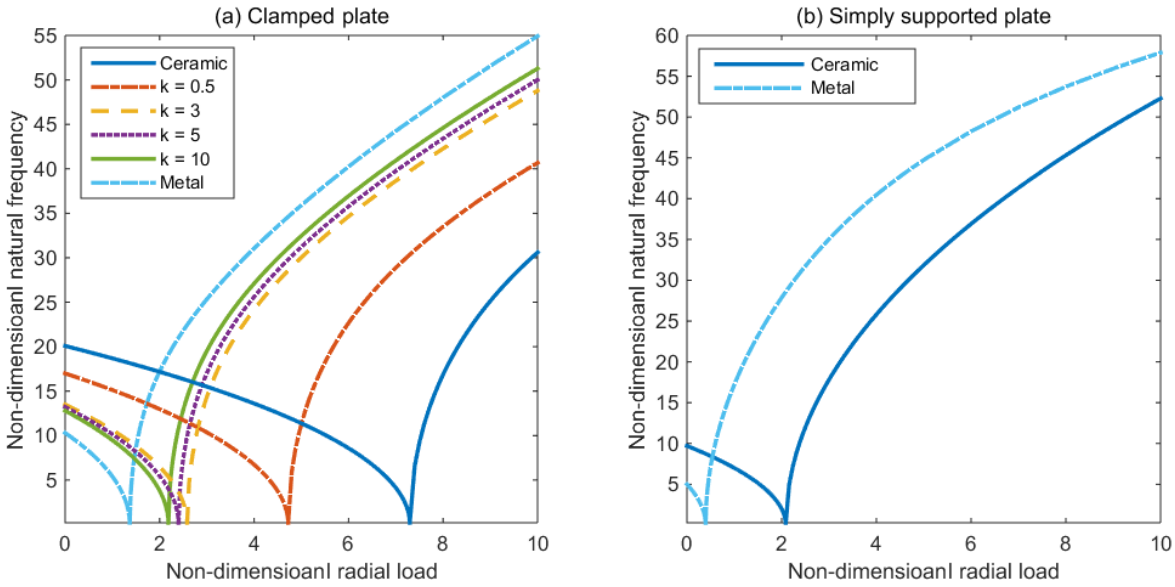

Fig. 7: Non-dimensional first natural frequency of the circular plate around the prebuckled and the first postbuckled configuration against non-dimensional radial load

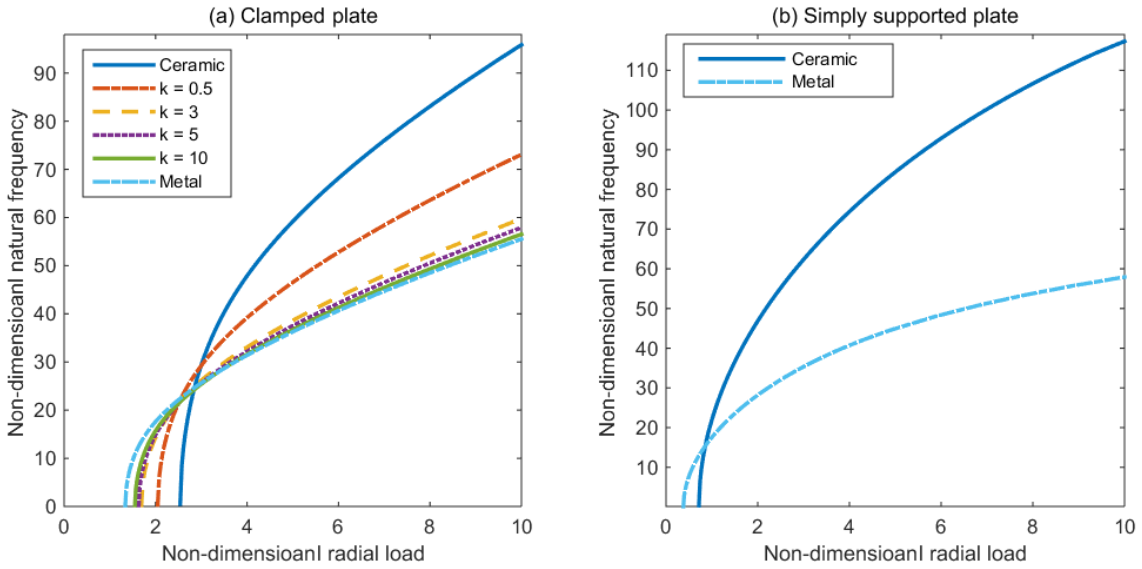

Fig. 8: Non-dimensional first natural frequency of the circular plate around the first postbuckled configuration against non-dimensional radial load

Table 1. Validation of the critical buckling load ($\times 10^6\ N/m$) of the clamped functionally graded circular plates

k	$\frac{h}{R} = 0.01$			$\frac{h}{R} = 0.03$			$\frac{h}{R} = 0.05$		
	Present work	CPT [2]	FSDT [2]	Present work	CPT [2]	FSDT [2]	Present work	CPT [2]	FSDT [2]
0	0.5109	0.5108	0.5107	13.7946	13.7927	13.7495	63.8639	63.8553	63.3022
0.5	0.3312	0.3311	0.3310	8.9422	8.9410	8.9161	41.3992	41.3937	41.0741
2	0.1987	0.1987	0.1986	5.3653	5.3646	5.3502	24.8394	24.8360	24.6523

Table 2. Validation of the lowest four non-dimensional linear natural frequencies of axisymmetric vibration of the clamped functionally graded circular plates

k	$\bar{\omega}_1$		$\bar{\omega}_2$		$\bar{\omega}_3$		$\bar{\omega}_4$	
	Present work	[3]	Present work	[3]	Present work	[3]	Present work	[3]
0.5	17.4693	17.2985	67.8710	67.0527	151.5222	-	267.6454	-
0.8	15.7946	16.0439	61.3647	62.0397	136.9968	-	241.9877	-
1	15.0869	15.4879	58.6160	59.8276	130.8633	-	231.1607	-
5	12.0604	12.4211	46.8706	48.1363	104.6935	-	185.0650	-
10	11.3981	11.5676	44.2992	45.0113	98.9592	-	174.9531	-
Metal	10.2483	10.2160	39.8305	39.7710	88.9767	89.104	157.304	158.181

Biographies

Abolfazl Shahabodini has received his MSc and PhD degrees in Mechanical Engineering from University of Guilan, Iran in 2017. At present, he is working as an Assistant Professor at the Department of Mechanical Engineering, Vali-e-Asr University of Rafsanjan, Iran. He has authored more than 20 publications in international journals and conferences. His main research interests include structural dynamics, nanomechanics, multiscale simulations and mechanism design.

Milad Saadatmand has received his BSc and MSc degrees in Mechanical Engineering from state universities in Iran. Currently, he is doing his PhD in building engineering at Concordia University, Montreal, Canada. His research interests include linear and nonlinear vibration and acoustic, modelling MEMS/NEMS sensor and actuators. Besides his research activities, he has teaching experiences in Iranian academic institutes and universities during 2013 to 2016. Furthermore, in 2016 he had a successful collaboration with center for acoustic-mechanical micro systems (CAMM) in Technical University of Denmark (DTU) as a research visitor.

Bahman Ahmadi has received his MSc and PhD degrees in Mechanical Engineering from University of Guilan, Iran. At present, he is working as an Assistant Professor at the department of mechanical engineering, University of Kurdistan, Iran. He is currently interested in game theoretic design, engineering optimization, and artificial intelligence.

Saeed Nezamivand Chegini has received his PhD degree in Mechanical Engineering from University of Guilan, Iran in 2019. He is currently the post doctora researcher at Shaheed Beheshti University. His research interests are applied mathematics for signal processing approaches, wavelet transform, optimization algorithm, rotating machinery fault detection and prognostics techniques. He wrote several international papers for Applied Soft Computing, Soft Computing, Measurement and Meccanica journals.